Designing Patterned Surfaces by Grafting Y-Shaped Copolymers

Ekaterina Zhulina* and Anna C. Balazs*

Department of Materials Science and Engineering, University of Pittsburgh, Pittsburgh, Pennsylvania 15261

Received September 15, 1995; Revised Manuscript Received January 11, 1996[⊗]

ABSTRACT: We use scaling arguments to determine the patterns that form when Y-shaped AB copolymers are grafted onto a flat surface. One "arm" of the Y is an A homopolymer, and the other arm is an incompatible B chain, and the short "stem" tethers the entire copolymer to the surface. We investigate the behavior of the brush formed from these chains in the melt and in the presence of a solvent. In particular, we determine how solvent quality, grafting density, and chain length affect the structure of the grafted layer. We then calculate a phase diagram that delineates the regions where the different structures appear. The diagram reveals that variations in the solvent quality give rise to a rich variety of lateral structures. The results provide guidelines for fabricating patterned or highly ordered thin films.

Introduction

The behavior of grafted polymers can be exploited to create thin films that contain well-defined structures or patterns. A current technological goal is to gain control over the size and features of such polymer films.[1] By taking advantage of the chemical composition, molecular weight, and the phase behavior of the grafted chains, one can design coatings that contain lateral patterns with the desired dimensions. These grafted layers are particularly useful in a variety of optoelectronic devices and provide a means of manipulating the size scale of the surface structures.

Through the aid of mean field theories[2,5,8] and computer simulation,[3,4,6−8] previous researchers observed a variety of patterns within the grafted layers as a function of the composition of the chains. In particular, investigators examined the behavior of a brush that contained a 50/50 mixture of incompatible homopolymers, A and B.[2−4] They predicted the formation of a "rippled" phase, where the polymers undergo a lateral phase separation into distinct A-rich and B-rich domains. In addition, Dong et al.[5] observed distinct patterns of phase separation in brushes composed of grafted diblocks. Unique structures have also been noted in polymer brushes where attractive functional groups are attached to the free ends of the chains.[6,7] In this case, a "layering" effect is observed: the functional groups are localized in a layer at the top of the brush. Gersappe et al.[8] varied the sequence distribution of tethered AB copolymers and found that brushes composed of blocky copolymers show distinct lateral inhomogeneities, with large, well-defined domains of A and B monomers. These domains appear diminished in size within the random copolymer brushes and disappear for brushes composed of alternating copolymers.

In this paper, we use theoretical models to determine the patterns that form when Y-shaped AB copolymers are grafted onto the surface. We consider the stem of the Y to be just one site in size and it serves to tether the macromolecule to the surface. We further assume that one arm of the Y is an A homopolymer, while the other arm is an incompatible B chain.[9] Recently, Dong examined a melt, or dry brush, of A and B homopolymers that were grafted in an alternating pattern (ABABAB...) on a surface.[10] He noted that heterogeneities in the layer would be easier to observe experimentally if the A and B chains were actually tethered to each other, as well as to the surface. It is this particular architecture that we examine here. We, however, go beyond the dry brush regime and determine how the presence of solvent, the grafting density, and chain length affect the morphology of the layer. As demonstrated below, the variations in the solvent quality give rise to a rich variety of lateral structures within the film.

Below, we summarize the salient features of our model and describe how we use scaling arguments to derive free energy expressions for the grafted layer. We then calculate a phase diagram that delineates the regions where the different structures appear.

The Model

The A and B branches of the Y-shaped copolymers are assumed to be flexible and identical in length: each branch contains $N \gg 1$ monomers. The size of each monomer is given by a and the junction point or stem of the Y is also of size a. The grafting density of the copolymers is $(1/s)$, where s is the area per branch. The chains are immersed in a solvent and the solvent quality is characterized by the value of the second virial coefficient, v_0a^3, in the expression for the free energy of mixing. (We consider the value of the third virial coefficient, wa,[6] to be independent of the temperature, a fact that we will use in later calculations described below.) We assume the solvent is nonselective; i.e., it is of the same quality for both components A and B. When $v_0N^{1/2} \gg 1$, the surrounding solution behaves as a good solvent; for $v_0N^{1/2} \ll -1$, the solution acts as a poor solvent and in the range $-1 \ll v_0 N^{1/2} \ll 1$, the solution provides Θ solvent conditions. The value of the Flory−Huggins interaction parameter, χ (>0), characterizes the incompatibility between the two blocks. As noted above, we vary the concentration of grafted chains and consider the behavior of the chains at both high and low grafting densities.

We first consider the case where the grafting density is relatively high and the height or thickness of the brush (which indicates the stretching of the chains in the direction normal to the surface) is given by $H = Na^3/s > aN^{1/2}$. To investigate this regime, we adopt a simple "box" model, similar to that used by Dong.[10] In particular, we assume that the brush is subdivided into two horizontal sublayers of thickness H_1 and $(H - H_1)$,

[⊗] Abstract published in *Advance ACS Abstracts,* March 1, 1996.

0024-9297/96/2229-2667$12.00/0

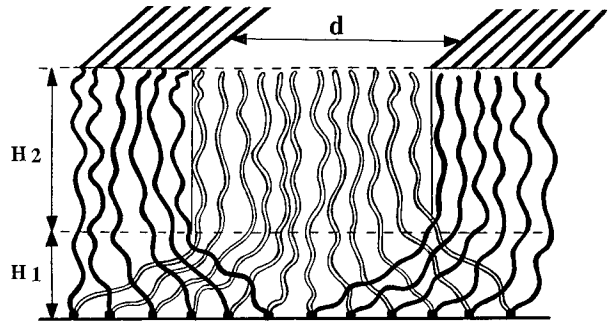

Figure 1. Laterally microsegregated brush formed by Y-shaped block copolymers.

respectively (see Figure 1). The lower sublayer is adjacent to the grafting surface and contains randomly mixed segments of the A and B chains. We further assume that the upper sublayer consists of microsegregated domains of A and B, which form regular, alternating "stripes". The width of each stripe is given by d and thus, the periodicity of the system is $2d$. Since the length of the A and B blocks are identical ($N_A = N_B = N$) and the solvent is nonselective, the concentrations of A and B units in the lower sublayer are equal: $c_A = c_B = c_1/2$, where c_1 is the total concentration (volume fraction) of polymer in this sublayer. In the upper sublayer, $c_A = c_B = c_2$ within the corresponding stripes, given that c_2 is the total concentration of polymer in the upper sublayer. We let $n = (c_1 s H_1)$ and $(N - n) = (c_2 s(H - H_1))$ denote the average number of units per block localized in the lower and upper sublayers, respectively.

Our model implies that the system undergoes a lateral microsegregation, which is preferable in the case of high molecular weight blocks and equal polymer–surface interaction parameters, $\chi_{AS} = \chi_{BS}$. However, when $\chi_{AS} \neq \chi_{BS}$, one can envision another scenario, i.e., a vertical segregation of the system. Here, the component with the more attractive surface interaction spreads on the grafting surface, and the second component forms a horizontal layer on top of the first. For the chains in the upper layer, the segments near the surface are strongly stretched, especially for $N \gg 1$. The losses in the total free energy can, however, be diminished by a gain in the surface free energy, provided that $\chi_{AS} \neq \chi_{BS}$. Thus, we do not exclude the possibility of a vertical segregation in that case. In this paper, however, we consider the "symmetric" situation where the A and the B blocks interact in a similar manner with both the solvent and the surface.

At low grafting densities, the brush loses its lateral homogeneity and splits onto separate coils in good or Θ solvents or aggregates into "pinned micelles" or "octopus" structures in poor solvents.[11,12] In considering this regime, we focus on the poor solvent conditions and consider pinned micelles formed by Y-shaped block copolymers. To carry out this investigation, we utilize the model of a pinned micelle introduced independently by Klushin[11] and Williams.[12] According to ref 11, a pinned micelle in a poor solvent has a well-defined structure, consisting of a "core" and "legs" connecting the core to the surface. The segments of the chain within the core are collapsed, while the segments in the legs are strongly stretched.

Additional features of these models are explained in the appropriate sections. We start by considering the behavior of the chains at high grafting densities. In particular, we isolate the effect of solvent by contrasting the properties of a melt of tethered polymers with a polymer brush immersed in a solution.

Results and Discussion

1. The Melt Regime. We start our investigation with the case of a grafted layer in the melt regime: $c_1 = c_2 = 1$. At relatively high grafting densities ($s/a^2 < N^{1/2}$), the segments in both sublayers are stretched in the direction normal to the underlying surface. In addition, the n segments in the lower sublayer stretch in the lateral direction, enabling the fragments in the upper layer to self-assemble into well-defined stripes (see Figure 1). The total elastic energy (per block) scales as

$$F_{el}/kT = H_1^2/(a^2 n) + d^2/(a^2 n) + (H - H_1)^2/(a^2(N - n)) \quad (1)$$

Here and throughout the paper, we will use an = sign in our equations; however, all numerical coefficients are omitted from these expressions (unless otherwise noted). Since the brush is in the melt regime, $H_1 s = na^3$ and $(H - H_1)s = (N - n)a^3$, which reduces eq 1 to

$$F_{el}/kT = H^2/(a^2 N) + d^2/(a^2 n) \quad (2)$$

The first term in eq 2 describes the normal stretching of the blocks in the brush, whereas the second expression accounts for the lateral stretching of the segments in the "mixed" (lower) sublayer.

Unfavorable contacts between A and B ($\chi > 0$) monomers are localized in the "mixed" sublayer and at the boundaries between the stripes in the upper sublayer. These interactions give rise to the following contributions in the free energy

$$F_{int}/kT = \chi n/4 \quad (3)$$

and

$$F_s/kT = \gamma_o s' \quad (4)$$

where s' is the area of contact per chain in a stripe and is related to N, n, and d as

$$s' = (N - n)a^3/d \quad (5)$$

and $\gamma_o = (\chi/6)^{1/2}/a^2$ is the surface free energy per unit area at the interface between the pure A and B components. Note that there is an additional surface contribution at the very outer boundary (top) of the brush

$$F'_s/kT = \gamma_o' s \quad (6)$$

where γ_o' is the corresponding surface tension. The total free energy per block is, thus, given by

$$F/kT = H^2/(a^2 N) + \gamma_o' s + d^2/(a^2 n) + \gamma_o(N - n)a^3/d + \chi n/4 \quad (7)$$

Minimizing F with respect to the two unknown parameters, n and d, yields the equilibrium parameters of the microsegregated state of the brush:

$$n = N^{1/2}/\chi^{1/2} \quad (8)$$

$$H_1 = aN^{1/2}/(s\chi^{1/2}) \quad (9)$$

$$d = aN^{1/2} \quad (10)$$

and substituting these terms back into eq 7 yields

$$F/kT = Na^4/s^2 + \gamma_o' s + (\chi N)^{1/2} \quad (11)$$

The last term in eq 11 accounts for unfavorable interac-

tions in the laterally segregated state of the brush, whereas the first two terms are the same as in the laterally homogeneous system. It is interesting to note that a variation of χ in this microsegregated state affects the values of n, H_1, and F but does not affect the value of $d = aN^{1/2}$. An increase in χ results in an increase in the thickness of the segregated sublayer and a corresponding decrease in the thickness of the "mixed" sublayer at the fixed value of the lateral periodicity, d.

The scaling dependences in eqs 9 and 10 were obtained earlier by Dong,[10] who used a more complex model. Our results, obtained with a simpler treatment, indicate that these features reflect rather general characteristics of the system, regardless of the particular details of the model.

2. Effects of Solvent. To formulate an expression for the effect of solvent on the system, we perform a heuristic or gedanken "experiment" where we take the melt case above and immerse this brush for a short time into a bath of solvent. We then remove the brush. We assume that the brush absorbs a fixed concentration of solvent. We further assume that the incompatibility between the blocks is relatively weak and does not affect the distribution of solvent throughout the brush, so that $c_1 = c_2 = c$, where c is the total concentration (volume fraction) of polymer units in the brush.

The interaction between the solvent molecules and polymer units can be described within the framework of a virial expansion, provided that $c \ll 1$. The Flory picture of polymer solutions[13] gives the free energy per chain as

$$F_{conc}/kT = Nvc + Nwc^2 + ... \qquad (12)$$

where

$$v = (1/2 - \chi_{PS}) + \chi/4 = v_0 + \chi/4 \quad \text{and} \quad w = 1/6 \qquad (13)$$

Here, $v_0 = (1/2 - \chi_{PS})$ accounts for the polymer−solvent interactions (χ_{PS} is the Flory−Huggins interaction parameter), whereas the second term in eq 13 is due to the unfavorable A−B interactions. Below, we consider relatively dilute systems where only the first two terms in the virial expansion, eq 12, are relevant. We also assume that $\chi \ll |v_0|$, which is often the case. This inequality allows us to consider the polymer−polymer interactions as a weak perturbation to the stronger polymer−solvent interactions and justifies the assumption of a nearly uniform distribution of solvent throughout both sublayers.

In this situation, we can replace χ by the product χc. In other words, the presence of solvent diminishes the number of monomer−monomer contacts (relative to the number in the melt) and the number of such contacts is just given by the volume fraction of monomer sites. In a similar manner, s is replaced by sc in our new scenario and the total thickness of the brush scales as $H = Na^3/sc$. Substituting these new terms into eqs 8, 9, and 11 yields the following new expressions:

$$n = (N/\chi c)^{1/2} \qquad (14)$$

$$H_1 = N^{1/2}/(s\chi^{1/2}c^{3/2}) \qquad (15)$$

and with the addition of eq 12 yields

$$F/kT = (\chi Nc)^{1/2} + Na^4/(sc)^2 + N(v_0 c + wc^2 + ...) + \gamma_o'(c)s \qquad (16)$$

As can be seen, introducing a fixed concentration of uniformly distributed solvent molecules leads to an increase in both the thickness and the relative volume of the first sublayer: in particular, $H_1 \sim c^{-3/2}$ and $H_1/H \sim (N\chi c)^{-1/2}$. However, the periodicity d is not sensitive to the value of χ and is the same as in the melt regime.

We can now use eq 16 to determine the equilibrium behavior of a brush in contact with an infinite reservoir of solvent. We can neglect the demixing contribution to this free energy, $F/kT \sim (\chi Nc)^{1/2} \sim N^{1/2}$, since this term is small with respect to the terms in the virial expansion and the chain stretching energy (which scales as N). We can also neglect the interfacial tension, $\gamma_o'(c)s$, since this term is zero in both good and Θ solvents and in poor solvents is negligible with respect to the other terms. The equilibrium concentration, c^*, is then determined by evaluating the expression $dF/dc = 0$. We can, however, further simplify eq 12 to reflect the nature of the surrounding solvent. In particular, for a good solvent, we can neglect the term (Nwc^2) in eq 12 and obtain the following relationship for c^*:

$$c = (v_0 s^2)^{-1/3} \qquad (17)$$

To determine the behavior in a Θ solvent, we can neglect the (Nvc) term in eq 12 and find that

$$c^* = (ws^2)^{-1/4} \qquad (18)$$

Finally, to find c^* in a poor solvent, we neglect the contribution from the stretching energy, $Na^4/(sc)^2$, (since the chains are relatively collapsed in a poor solvent) and obtain

$$c^* = |v_0|/w \qquad (19)$$

The equilibrium value of the demixing term, $F'/kT = (\chi Nc^*)^{1/2}$, determines whether the swollen brush is microsegregated or not. For a brush with randomly mixed components A and B, the loss in the free energy due to the unfavorable A−B contacts scales as

$$F'_r/kT = \chi Nc^* \qquad (20)$$

whereas all other contributions (normal elastic stretching of blocks, solvent−polymer interactions and the surface energy at the edge of the brush) are the same as for a microsegregated brush. Thus, comparing F' and F'_r, one gets that at $\chi Nc^* \gg 1$ the brush is microsegregated, whereas at $\chi Nc^* \ll 1$ it is expected to be in the laterally homogeneous (randomly mixed) state.

In the remaining portions of the paper, we focus on the case of poor solvents ($v_0 < 0$). In this regime, the chains can undergo lateral segregation and coupling this phase behavior with an incompatibility between the tethered copolymers can further drive the chains to form a variety of unique morphologies. We first consider the case where the incompatibility of the blocks is relatively weak and then examine the behavior between more incompatible chains.

3. Effects of Poor Solvents. A. Weakly Incompatible Blocks. To facilitate our discussion, we introduce the parameter τ, which is a measure of the relative deviation from the Θ temperature:

$$\tau = (\Theta - T)/\Theta = -v_0 > 0 \qquad (21)$$

As noted above (see eq 19), when the blocks are only weakly incompatible and the distribution of solvent is nearly uniform ($c_1 = c_2 = c^*$), c^* for a collapsed brush

does not depend on the grafting density $1/s$ and is determined by the values of the second and the third virial coefficients, v_0 and w. Substituting the expression for c^* into eqs 14−16 yields the equilibrium characteristics of a microsegregated brush in a poor solvent. In carrying out this substitution, we assume that the value of w is on the order of unity and is omitted from further consideration. Consequently, we arrive at the following relationships:

$$n = (N/\chi\tau)^{1/2} \tag{22}$$

$$H_1 = N^{1/2}s^{-1}\chi^{-1/2}\tau^{-3/2} \tag{23}$$

$$F/kT = -N\tau^2 + (\chi\tau N)^{1/2} + Na^4/s^2\tau^2 + \gamma_o'(\tau)s \tag{24}$$

where $\gamma_o'(\tau) \sim \tau^2/a^2$ is the surface tension at the boundary between the collapsed polymer brush and the pure solvent.[14,15] The value of d, which characterizes the periodicity of the structure, is still given by eq 10. Again, we note that all numerical coefficients are neglected in the actual expression and in the discussion of the expression below.

To understand the significance of each term in eq 24, it is helpful to picture the brush as a densely packed system of thermal blobs.[14,15] Each blob is of size $\zeta = a/\tau$ and contains $\zeta^2/a^2 = \tau^{-2}$ monomers. The free energy of the polymer−solvent interactions per blob is on the order of $-kT$. The total free energy of the polymer−solvent interactions per block is then given by the total number of blobs in a block, $=-N\tau^2$, or the first term in eq 24.

The blobs in the different, incompatible blocks experience a repulsive interaction that is $+(\chi/\tau)kT$ per blob. In the first sublayer, each block contains $n_b = n\tau^2$ blobs, and the volume fractions of the A and B blobs are equal. Thus, one gets for the repulsive contribution $n_b(\chi/\tau) = n\chi\tau = (\chi\tau N)^{1/2}$, or the second term in eq 24.

In the second sublayer, there are additional contacts between chemically distinct blobs at the boundaries between the stripes (see Figure 1). The thickness of these boundaries is given by $\Delta = a/(\chi\tau)^{1/2}$. The loss per block due to these contacts can be estimated as $\Delta\chi s'/\tau\zeta^3 = (\chi\tau N)^{1/2}$, where $s' = (Na^3/d\tau)$ is the area of the interface per block. Thus, the contribution to the free energy from these border interactions is of the same order of magnitude as that in the mixed (first) sublayer.

The elastic stretching of a chain of blobs in the normal direction is taken into account by the third term in eq 24. Note, that the entropic losses due to the lateral stretching of the n-segments in the first sublayer, $d^2/na^2 = (\chi\tau N)^{1/2}$, are of the same order of magnitude as the energetic interactions between the blobs on the borders of the stripes and are therefore represented by the second term of eq 24.

Finally, the last term in eq 24 takes into account the loss of free energy at the outer edge of the brush. The thickness of the boundary between the brush and the pure solvent is on the order of magnitude of the blob size ζ, and thus, one can estimate these losses as the number of blobs at the outer edge of the brush, s/ζ^2.

B. Highly Incompatible Blocks. Equations 22−24 are valid under the conditions that $\tau \gg (s/a^2)^{-1/2}$ and $\chi \ll \tau$. The A and B blocks, however, may be highly incompatible, yielding the condition that $\chi \gg \tau$. The segments closest to the junction point between the A and B blocks are expected to be the most affected by a strong repulsion between the chains. Near these sites, the chains stretch away from each other to avoid the unfavorable contacts (a point that we will discuss further below). This behavior effectively decreases c_1, the volume fraction of polymer in the first sublayer. Far away from the junction point, within the second sublayer, the A and B polymers are already separated into stripes and an increase in χ affects only the boundary regions between the stripes. That is, the concentration of polymer within the stripe is unaffected. Consequently, the concentration of polymer in this layer, c_2, remains $\approx c^* \approx \tau$.

In this scenario, the solvent molecules are no longer uniformly distributed within the brush. In particular, the solvent is concentrated in the first sublayer and at the boundaries between the stripes. In the latter region, the solvent effectively diminishes the number of A−B interactions by replacing the unfavorable polymer contacts with polymer−solvent contacts. These solvent effects contribute to the free energy (per block), which can be written as

$$F/kT = (N - n)a^4/(s\tau)^2 + na^4/(sc_1)^2 + d^2/na^2 - (N - n)\tau^2 + n(vc_1 + c_1^2 + ...) + aN\tau/d + s\tau^2 \tag{25}$$

where, as before, all numerical coefficients are omitted. The first two terms account for the normal stretching, while the third term describes the lateral stretching of the chains. The two subsequent terms arise from the virial expansion (which we will subsequently refer to as the "volume" interactions) for both sublayers. Of the last two terms, $(N\tau/d)$ arises from the polymer−solvent interactions at the boundaries of the stripes. The last term describes the surface tension between the top of the brush and the solvent (see eq 24 and the subsequent line). Using the inequalities $\chi \gg \tau$ and $c_1 \ll \tau$, eq 25 can be simplified as

$$F/kT = \text{Const}(c_1,d,n) + na^4/(s\tau)^2 + d^2/na^2 + n(\tau^2 + \chi c_1) + aN\tau/d \tag{26}$$

where we collected all the terms independent of c_1, d, and n into Const(c_1,d,n). Minimizing F with respect to c_1, d, and n gives the following relationships

$$c_1 = s^{-2/3}\chi^{-1/3} \tag{27}$$

$$d = a(nN\tau)^{1/3} \tag{28}$$

$$n = d/a[\tau^2 + (\chi/s)^{2/3}]^{1/2} \tag{29}$$

Equations 27−29 characterize the structure of the brush at $\chi > \tau$. As follows from eq 29, in the range $\tau \ll \chi \ll s\tau^3$,

$$n = d/a\tau = N^{1/2}/\tau \tag{30}$$

One can envision the n-segments in this range of parameters as laterally stretched strings of blobs, so that

$$d = n_b\zeta = an\tau \tag{31}$$

The repulsive interaction between the strings of A and B blobs leads to an additional stretching in the normal direction, so that the concentration of polymer units $c_1 < \tau$ (see eq 27). One can use the following arguments to clarify the scaling dependence in eq 27. Each chain of n_b blobs has on average $n_b\Phi_b$ heterocontacts between blobs, where $\Phi_b = c_1/\tau$ is the volume fraction of blobs in the first sublayer. Each heterocontact costs $(\chi/\tau)kT$. The

total loss of free energy of heterocontacts per block scales as $n_b\Phi_b(\chi/\tau)$, whereas the elastic free energy of the chains of blobs scales as $H_1^2/n_b\zeta^2 = n_b\zeta^4/s^2\Phi_b^2$. The balance of these two terms gives $\Phi_b = (s^2\chi\tau^3)^{-1/3}$ and, correspondingly, the dependence in eq 27 for the polymer concentration. Thus, in the range of $\tau \ll \chi \ll s\tau^3$, the stretching of the chains of blobs in the lateral direction is combined with a normal stretching. (This behavior is reminiscent of that for a brush in a good solvent.[16]) Here H_1 increases with increasing χ as

$$H_1 = na^2/sc_1 = N^{1/2}\chi^{1/3}/\tau s^{1/3} \tag{32}$$

whereas the periodicity parameter, d, is still given by eq 10.

In the limit where the blocks are highly incompatible, or $\chi \gg s\tau^3$, eq 29 gives

$$n = d(s/\chi a^2)^{1/3} \tag{33}$$

and one gets from eqs 28 and 33

$$d = N^{1/2}(s\tau^3/\chi)^{1/6} \tag{34}$$

$$n = N^{1/2}(s\tau/\chi)^{1/2} \tag{35}$$

Correspondingly, the thickness of the first sublayer scales in this regime as

$$H_1 = n/sc_1 = N^{1/2}(s\tau^3/\chi)^{1/6} = d \tag{36}$$

By comparing the above with eq 32, it is clear that at extremely strong incompatibilities of A and B ($\chi \gg s\tau^3$), the representation of the n-segments as strings of blobs is no longer valid: highly repulsive hetero-interactions destroy the local structure of the blobs. Here, the periodicity of the structure, d, diminishes with increasing χ. It is interesting to note that the dependence of H_1 on χ is not monotonic. It passes through a minimum in the vicinity of $\chi \sim \tau$ and passes through the maximum at $\chi \sim s\tau^3$. However, this range of χ values is hardly attainable in realistic situations.

Having determined the properties of the system in the brush or high grafting regime, we also examine the behavior of these tethered Y's at lower grafting densities. We will confine our discussion to the poor solvent case. As above, we consider both cases: weakly and highly incompatible blocks.

4. Low Grafting Densities or the "Sparse Brush" Regime. For densely grafted polymers, the chains are stretched beyond their Gaussian dimensions, i.e., $s/a^2 \ll N^{1/2}/c^*$. Normally, decreasing the grafting density (or equivalently, increasing s) leads to a weakening of the demixing interactions between the polymers and, therefore, a stabilization of the homogeneous state. This observation, however, is only true when $\chi = 0$ and the loosely grafted chains are in a good or Θ solvent. At low grafting densities and in poor solvents, the brush splits into "pinned micelles" and forms a laterally inhomogeneous layer. This occurs even when $\chi = 0$.[11]

Here, we consider the case of a poor solvent and a range of areas $s > N^{1/2}/c^*$, where $c^* \sim \tau$ is the equilibrium swelling concentration in a collapsed state. Under these conditions, the chains aggregate into micelles that consist of a spherical core of the radius R and "legs" that connect the core to the surface (see Figure 2). The total area of the micelle is given by $D^2 = fs$, where f is the number of chains in a micelle. Each leg consists on average of $n \ll N$ units and is strongly stretched.

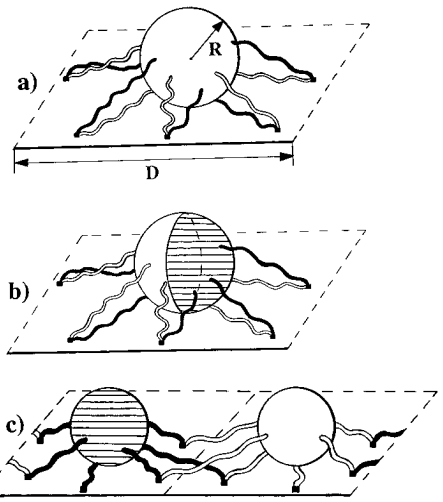

Figure 2. Pinned micelles formed by Y-shaped block copolymers: (a) mixed micelles; (b) internally segregated micelles; (c) split micelles.

Within the core, the concentration of polymer is c^*, so that

$$R = a(fN/\tau)^{1/3} \tag{37}$$

In the absence of demixing interactions, or $\chi = 0$, the free energy per block in such a structure is

$$F/kT = D^2/na^2 - (N - n)\tau^2 + \gamma_o'(\tau)R^2/f = sf/na^2 - (N - n)\tau^2 + N^{2/3}\tau^{4/3}/f^{1/3} \tag{38}$$

The first term describes the lateral stretching of the legs, the second term accounts for the volume interactions in the core of the micelle, and the last term represents the loss of free energy at the outer surface of the core.

Minimizing F with respect to n and f gives

$$n = D/\tau \tag{39}$$

$$f = N^{4/5}\tau^{2/5}a^{6/5}s^{-3/5} \tag{40}$$

$$D = aN^{2/5}(\tau s/a^2)^{1/5} \tag{41}$$

$$R = aN^{3/5}(\tau s/a^2)^{-1/5} \tag{42}$$

and, finally,

$$F/kT = -N\tau^2 + N^{2/5}(s/a^2)^{1/5}\tau^{6/5} \tag{43}$$

Once again, we can use the concept of blobs to describe the structure of the pinned micelles. The core of the micelle is densely packed with blobs, while the legs are totally stretched strings of blobs. Thus, in the range of low grafting densities, $s/a^2 \gg N^{1/2}/\tau$, one finds a laterally inhomogeneous state of the brush, which contains polymer-rich domains (the core of the micelles) and solvent-rich regions (in the vicinity of the stretched legs).

A. Weakly Incompatible Blocks. Introducing demixing interactions between the A and B blocks ($\chi > 0$) favors the appearance of additional inhomogeneities within the grafted layer. Since the majority of the monomers are localized in the cores of the micelles, the effects of an A−B repulsion will first manifest themselves in the core. For values of χN below a critical value ($\chi N \ll (\chi N)^*$), the A and B blocks are randomly mixed within the core; however, for $\chi N \gg (\chi N)^*$ the A and B blocks inside each core will segregate. These structures are drawn schematically in Figure 2a,b,

respectively. We can estimate the value of $(\chi N)^*$ by using the following arguments. Segregation of the A and B blocks leads to the appearance of a boundary between the A and B parts in the core (see Figure 2b). The area of the boundary, S, scales as R^2 (where R is the radius of the micelle) and the resulting surface tension at this boundary is given by $\gamma_o(\tau) = \gamma_o\tau^{3/2}$ (where we made use of the known result[17] that $\gamma_o(c) = \gamma_o c^{3/2}$ and the fact that $c = \tau$). Thus, due to this boundary, one has

$$F_s/kT = \gamma_o\tau^{3/2}R_o^2/f \tag{44}$$

per block in the core. Balancing F_s with the free energy of randomly mixed A and B blocks,

$$F_{mix}/kT = N\chi\tau \tag{45}$$

one gets the transition point between the mixed and demixed states of the micellar core,

$$(N\chi\tau)^* = (s\tau/N^{1/2})^{2/5} \tag{46}$$

Above this point, the core is "polarized", the A and B blocks are segregated inside the core (Figure 2b), whereas below this point, the A and B units are randomly mixed (Figure 2a).

B. Highly Incompatible Blocks. When χ is above the critical value described above but, nonetheless, $\ll\tau$, the loss in free energy at the A−B boundary within the micelle (see Figure 2b) is less than that at the outer surface of the core. Consequently, the internally demixed micelle is stable with respect to the total segregation of A and B components. However, when $\chi \gg \tau$, splitting of the original micelle into two separate micelles, each composed of pure A or B, becomes more favorable. The structure of this system is drawn in Figure 2c. The equilibrium parameters of each micelle (A and B) are still described by the scaling dependences in eqs 39−42. However, the numerical prefactors in these dependences change (diminish) and each micelle contains fewer chains than the original, common micelle. Since each block now has an area per chain of $2s$, instead of s as in a common micelle, the number of chains, f, in each new micelle diminishes by a factor of $2^{-3/5}$ (see eq 40).

Splitting into micelles of pure A and B diminishes the unfavorable A−B contacts inside the cores, where the majority of these contacts were localized. Since the fraction of monomers in the legs is relatively low, their contribution to A−B interactions is small. However, at very high values of χ, the strong repulsion between the few A−B contacts in the legs can lead to a rearrangement of the micelles. In particular, when $\chi \gg \tau$, in order to diminish the number of such contacts, the legs start to stretch normal to the surface and thereby raise the height of the core. Let H_1 be the average height of the core above the surface and n, as before, is the number of units in a leg. At a given value of f, the legs give rise to the concentration $c_A = c_B = fn/D^2H_1$ between the core and the surface. Correspondingly, the free energy (per block) of unfavorable A−B contacts is given by

$$F_{int}/kT = \chi n^2/sH_1 \tag{47}$$

The elastic free energy of the legs is given by

$$F_{el}/kT = (D^2 + H_1^2)/na^2 \tag{48}$$

whereas the volume and the surface free energies of the core (per chain) are

$$F_{conc}/kT = -(N - n)\tau^2 \tag{49}$$

$$F_s/kT = (N - n)^{2/3}\tau^{4/3}/f^{1/3} \sim N^{2/3}\tau^{4/3}/f^{1/3} \tag{50}$$

The total free energy per block reads

$$F/kT = -N\tau^2 + n\tau^2 + (D^2 + H_1^2)/na^2 + \chi n^2/sH_1 + N^{2/3}\tau^{4/3}/f^{1/3} \tag{51}$$

Minimizing F with respect to H_1 and n gives

$$H_1 = a\chi^{1/3}n(a^2/s)^{1/3} \tag{52}$$

$$n = D/[\tau^2 + (\chi a^2/s)^{2/3}]^{1/2} \tag{53}$$

At $\tau \gg (\chi a^2/s)^{1/3}$ one gets

$$n = D/\tau \tag{54}$$

and, correspondingly, the scaling dependences in eqs 40−42 for the characteristics of the micelle. However, at $\tau \ll (\chi a^2/s)^{1/3}$, eq 53 gives

$$n = D(\chi a^2/s)^{-1/3} \tag{55}$$

and the scaling arguments depicting a leg as a string of blobs fail. Here, the legs become shorter (contain fewer monomers) and are more strongly stretched than the corresponding string of thermal blobs. Substituting eqs 52 and 55 into eq 51, one gets

$$F/kT = -N\tau^2 + D(\chi a^2/s)^{1/3} + N^{2/3}\tau^{4/3}s^{1/3}/D^{2/3} \tag{56}$$

Finally, minimizing F with respect to D gives the equilibrium parameters of the micelles in the limit of very high incompatibility,

$$D/a = N^{2/5}(\tau s/a^2)^{1/5}(s\tau^3/a^2\chi)^{1/5} \tag{57}$$

$$R/a = N^{3/5}(\tau s/a^2)^{-1/5}(s\tau^3/a^2\chi)^{2/15} \tag{58}$$

$$f = N^{4/5}\tau^{2/5}a^{6/5}s^{-3/5}(s\tau^3/a^2\chi)^{2/5} \tag{59}$$

$$H_1 = D \tag{60}$$

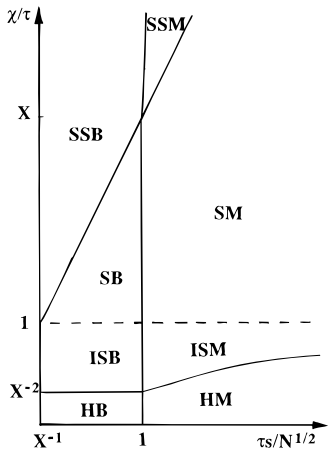

Figure 3. Diagram of states for the system in χ/τ, $\tau s/N^{1/2}$ coordinates, $X = \tau N^{1/2} \gg 1$. The various regimes indicated in the diagram are discussed in the text.

5. Diagram of States. Figure 3 represents a "diagram of states" for the system under poor solvent conditions. The ratios $y = \chi/\tau$ and $x = (\tau s/N^{1/2})$ are

chosen as the reduced variables. The diagram contains regions for a laterally homogeneous, mixed brush (HB) and homogeneously mixed micelles (HM), the regimes of segregated brushes (ISB, SB, and SSB) and the regimes of segregated micelles (ISM, SM, and SSM). As the diagram shows, a sparse grafting of block copolymers stabilizes the system against microphase segregation: the boundary between the regime of homogeneous micelles, HM, and the regime of internally segregated micelles, ISM, is located at higher values of χ/τ than for the corresponding brushes, regimes HB and ISB (internally segregated brush). This is due to the fact that the formation of a boundary between the A-rich and the B-rich phases is more unfavorable at sparse grafting. In this case, the losses per chain at the boundary increase with increasing s and higher values of χ are necessary to cause microphase segregation within pinned micelles (see eq 46).

The dashed line in Figure 3, $\chi/\tau = 1$, indicates the boundary between internally segregated micelles, containing both A and B components (regime ISM, $\chi/\tau < 1$), and split, pinned micelles of pure A and B components (regime SM, $\chi/\tau \geq 1$). For the brush regimes ISB and SB, this boundary corresponds to the penetration of pure solvent between the segregated A-rich and B-rich domains and substitution of the A−B boundaries by the A−S and B−S boundaries. (Here the letter S indicates the solvent.) Note that both above and below the dashed line, the characteristics of the system are given by the same power law dependences (eqs 10, 30, and 32 for the ISB and SB regimes and eqs 39−42 for the ISM and SM regimes) and differences can only be found in the numerical prefactors and nonpower dependences.

Above the dashed line, the A and the B blocks are separated to the maximal extent: the unfavorable contacts between A and B units are found only in the first sublayer for brushes and in the "coronas" for pinned micelles. The unfavorable contacts give rise to an additional stretching of the chain segments in the first sublayer of the brush and a stretching of the micellar legs normal to the surface. Above the boundary $\chi/\tau = s\tau^2$, these unfavorable A−B contacts also cause a rearrangement of the overall structure, diminishing the periodicity (regimes SSB and SSM, eqs 39 and 57). For relatively dense systems, where the concentration of the A−B contacts is relatively high (brush regime), this new regime is probably attainable. However, for sparse systems (pinned micelles regime), the values of $\chi > \tau N^{1/2}$ where the rearrangement of the micelles structure is expected is hardly attainable for conventional block copolymers. Thus, for realistic values of χ, one expects two main regimes of microsegregation at sparse grafting: internally segregated, "polarized" micelles or single-component, split micelles. In both regimes, the scaling laws (eqs 10, 30, and 32), indicate no power dependence of the relevant parameters on the value of χ. However, by varying the solvent quality, one can transfer the system from one regime into another and, thus, affect partial mixing or demixing of the A and B components in the system.

Conclusions

Our results demonstrate that Y-shaped grafted copolymers can form well-defined structures at both dense and sparse grafting. The presence of a third component, namely the solvent, enriches the set of possible structures and affects their stabilities. Even for the simplest case of a nonselective solvent (which we considered here), one finds a variety of structures, especially under poor solvent conditions.[20] Due to the interplay between unfavorable polymer−solvent interactions and the A−B repulsion, microphase segregation in such systems is governed not only by the molecular weights of the blocks and the value of χ but also by the grafting density. In particular, the mixed state of A and B blocks is more stable at sparse grafting (which is the typical case for most experimental situations) than at high grafting densities. Such findings provide guidelines for tailoring the morphology of the grafted layer for specific applications.

Further modification of the layer can be achieved by grafting asymmetric block copolymers (with different block lengths) and introducing selective solvents. Another option is to use a nonuniform or selective tethering of these chains onto the surface. Recent analysis[19] of selectively tethered homopolymers indicates that the morphology of the self-assembling structures is sensitive not only to the value of the grafting density but also to the shape of the underlying substrate. One expects similar effects for tethered, Y-shaped block copolymers. We will return to these questions in a forthcoming publication.

Acknowledgment. We thank Drs. John Rabolt and Greg Ferguson for enlightening discussions. A.C.B. gratefully acknowledges financial support from the Materials Research Center, funded by AFOSR, through grant number F49620-95-1-0167, and the DOE for financial support through grant DE-FG02-90ER45438.

References and Notes

(1) Committee on Polymer Science, National Research Council. *Polymer Science and Engineering: The Shifting Research Frontiers*; National Academy Press: Washington, DC, 1994.
(2) Marko, J. F.; Witten, T. A. *Macromolecules* **1992**, *25*, 296.
(3) Brown, G.; Chakrabarti, A.; Marko, J. F. *Europhys. Lett.* **1994**, *25*, 239.
(4) Lai, P. Y. *J. Chem. Phys.* **1994**, *100*, 3351.
(5) Dong, H.; Marko, J. F.; Witten, T. A. *Macromolecules* **1994**, *27*, 6428.
(6) Gersappe, D.; Fasolka, M.; Balazs, A. C.; Jacobson, S. H. *J. Chem. Phys.* **1994**, *100*, 1970.
(7) Li, W.; Balazs, A. C. *Mol. Simul.* **1994**, *13*, 257.
(8) Gersappe, D.; Fasolka, M.; Israels, R.; Balazs, A. C. *Macromolecules* **1995**, *28*, 4753.
(9) The behavior of brushes composed of Y-shaped homopolymers was investigated by: Szeifler, I. *Macromolecules* **1994**, *27*, 702. Here, the stem of the Y was longer than one lattice site.
(10) Dong, H. *J. Phys. II Fr.* **1993**, *3*, 999.
(11) Klushin, L. I. Preprint, 1992.
(12) Williams, D. R. M. *J. Phys. II* **1993**, *3*, 1313.
(13) Flory, P. J. *Principles of Polymer Chemistry*; Cornell University Press: Ithaca, NY, 1953.
(14) Williams, C.; Brochard, F.; Frish, H. L. *Annu. Rev. Phys. Chem.* **1981**, *32*, 433.
(15) Lifshits, I. M.; Grossberg, A. Y.; Khokhlov, A. R. *Rev. Mod. Phys.* **1978**, *50*, 6831.
(16) Alexander, S. *J. Phys.* **1977**, *38*, 983.
(17) Noolandi, J.; Hong, K. M. *Macromolecules* **1983**, *16*, 1443.
(18) Birshtein, T. M.; Zhulina, E. B. *Polymer* **1984**, *25*, 1453.
(19) Gross, N. A.; Zhulina, E. B.; Balazs, A. C. *J. Chem. Phys.* **1996**, *104*, 727.
(20) Though we only considered the case of a planar surface, we also expect to find a variety of structures on curved surfaces. For slightly curved surfaces, the general trends will be the same as those in the planar case. However, at highly curved surfaces, regimes with new scaling dependences are expected for both densely and sparsely grafted systems.[12,18]

MA951396F